JACS
JOURNAL OF THE AMERICAN CHEMICAL SOCIETY
Communication
pubs.acs.org/JACS
Terms of Use

Resonant Photocurrent Generation in Dye-Sensitized Periodically Nanostructured Photoconductors by Optical Field Confinement Effects

M. Anaya, M. E. Calvo, J. M. Luque-Raigón, and H. Míguez*

Instituto de Ciencia de Materiales de Sevilla (Consejo Superior de Investigaciones Científicas-Universidad de Sevilla), C/Américo Vespucio 49, 41092 Sevilla, Spain.

Supporting Information

ABSTRACT: Herein we show experimental evidence of resonant photocurrent generation in dye-sensitized periodically nanostructured photoconductors, which is achieved by spectral matching of the sensitizer absorption band to different types of localized photon modes present in either periodic or broken symmetry structures. Results are explained in terms of the calculated spatial distribution of the electric field intensity within the configurations under analysis.

Materials in which a spatial variation of the refractive index is built up in distances on the order of optical wavelengths display constructive and destructive interference effects between the reflected and transmitted beams at multiple interfaces.[1] This results in strong variations of the electric field intensity, which gives rise to reinforced matter−radiation interactions at specific locations within the structure.[2] Also, nanostructures can serve as supporting materials for other absorbing or optically active species,[3,4] usually providing large specific surface areas. In order to take advantage of both types of properties, nanostructures can in turn be arranged or patterned at submicrometer-length scale.[5−8]

Photoelectrochemical devices may largely benefit from the electromagnetic field localization occurring within periodic photonic nanostructures.[9] Different studies show that the efficiency is improved of both photocatalytic and photovoltaic cells when such materials, capable of enhancing radiation−matter interactions at specific locations and wavelengths, are introduced.[10−15] However, proofs of concept thus far reported are based on the observation of performance parameters, the improvement of which cannot be unambiguously linked to increased electron photogeneration resulting from optical field confinement and discriminated from diffuse scattering effects.[16−18]

In a stack of layers of photoconducting materials with alternated porosity,[19−23] the possibility opens up to modify the spectral response of the photocurrent by means of the optical design. However, the refractive index contrast is usually low, a large number of periods being required in order to observe strong Bragg scattering phenomena. This has prevented the observation of clear field confinement effects on the photocurrent spectrum of these multilayers so far. Alternative approaches based on inverse opal photoconducting structures lead to photonic crystal lattices with larger dielectric contrast but high density of intrinsic defects, which gives rise to strong diffuse scattering and weak Bragg reflections,[10,11,13,24] again being difficult to link the observed enhancement to specific photon resonances.

We have built both periodic and broken symmetry nanostructured photoconducting TiO_2 multilayers with enough number of periods as to display different types of photon resonances that confine the field within the material in different ways. Such modes were devised to match different spectral regions of the absorption spectrum of a dye, employed as a sensitizer, supported by the nanostructure. As in some heterojunction solar cells,[25] the large specific surface area of the porous nanostructure is used to obtain a high load of dye in a thin multilayered slab as well as to provide a means to inject and transport the electrons photogenerated at the dye. Two different synthesized TiO_2 nanocrystal suspensions were sequentially cast on a flat transparent conducting substrate by spin coating, leading to thin films of alternate refractive index, resulting from their different porosity. Full details of the preparation methods are provided in the Supporting Information [SI]. In Figure 1 field emission scanning electron microscopy (FESEM) images of cross sections of both periodic and broken translational symmetry multilayers are shown (a and b of Figure 1, respectively). For the latter, a wider, high-porosity middle layer was deposited to interrupt the periodicity. A higher magnification picture of this controlled defect or cavity is displayed in Figure 1c. Please notice that the number of unit cells is eight, higher than what has so far been reported for similar structures.[21,22] This leads to intense Bragg reflections clearly detectable in the transmittance spectra, which are shown in Figure 2. The periodic nanostructure displays a well-defined specular transmittance peak centered around λ_B = 520 nm (Figure 2a), surrounded by secondary lobes arising from the interference of beams transmitted at the top and bottom surface of the sample. The multilayer with a similar period, but embedding a midlayer of larger thickness to disrupt the periodicity, shows a reflection window in the middle of the photonic stop band, at around λ_C = 480 nm. Such a dip in the transmittance spectrum is the fingerprint of resonant modes localized within the consciously introduced defect layer that behaves as an optical cavity. In both cases, transmittance spectra were recorded at different incident angles, a clear blue-

Received: February 2, 2013
Published: May 7, 2013

   dx.doi.org/10.1021/ja401096k | J. Am. Chem. Soc. 2013, 135, 7803−7806

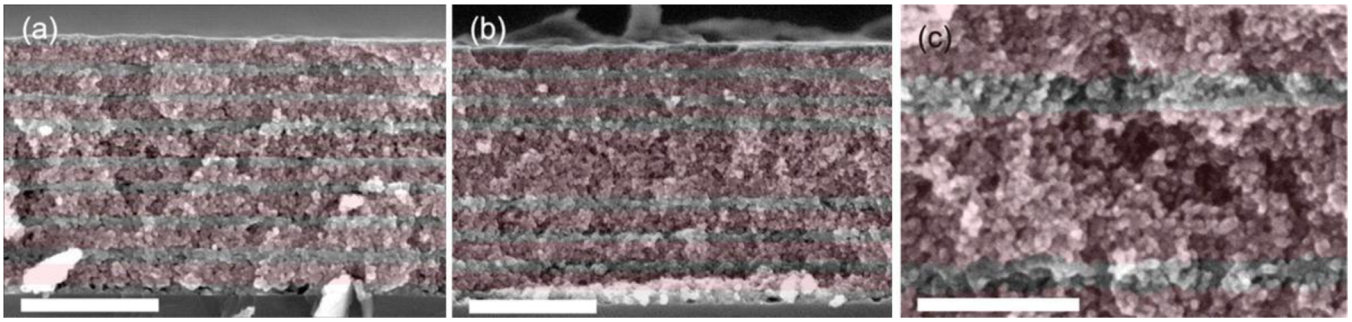

Figure 1. FESEM images of cross sections of (a) a periodic multilayer and (b) a multilayer in which a thicker middle layer has been deposited. (c) Higher magnification detail of this midlayer. Each type of layer has been shaded with a different color for the sake of clarity (gray, thinner lower porosity layer; purple, thicker higher porosity layer). Scale bars are 500 nm in (a) and (b) and 300 nm in (c).

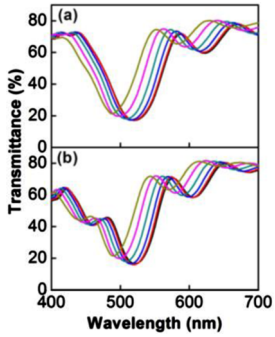

Figure 2. Transmittance spectra for different incident angles, 0° (black), 10° (red), 20° (blue), 30° (cyan), 40° (magenta), and 50° (dark yellow) of (a) a periodic multilayer (alternate TiO_2 layer thickness is d_1 = 90 nm and d_2 = 47 nm) and (b) a resonator built by depositing a thicker middle layer in a periodic multilayer (d_1 = 88 nm, d_2 = 44 nm, and defect layer d_3 = 240 nm). Refractive indexes are n_1 = 1.88 and n_2 = 2.12 in all cases, and $n_3 = n_1$.

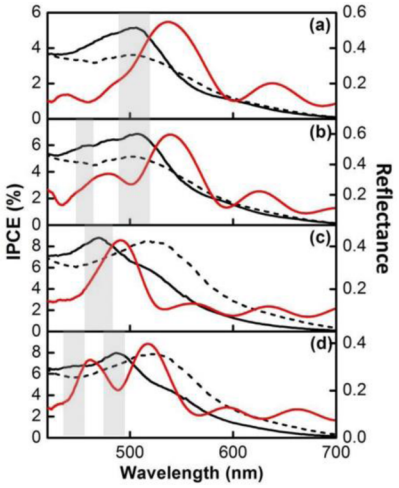

Figure 3. Incident photon to current efficiency (black solid lines) measured for dye-sensitized periodic multilayers: (a) (d_1 = 90 nm, d_2 = 47 nm) and (c) (d_1 = 81 nm, d_2 = 42 nm). Dye-sensitized multilayers in which a thicker middle layer has been deposited: (b) (d_1 = 88 nm, d_2 = 44 nm, d_3 = 240 nm) and (d) (d_1 = 81 nm, d_2 = 42 nm, d_3 = 262.5 nm). Black dashed lines represent IPCEs for designed TiO_2 reference cells for each sample. Refractive indexes are n_1 = 1.88 and n_2 = 2.12 in all cases, and in the middle layer $n_3 = n_1$. The reflectance measured from the photonic crystal electrode is also included (red solid lines). Shaded regions indicate the spectral position of resonances expected to enhance the photocurrent generation.

shift of all optical features being observed. Please notice that maximum transmittance achieved in the pass bands regions (λ > 600 nm) is ~80% instead of the 85−90% expected from simulations (see SI, Figure S1), which indicates the presence of structural defects in the multilayer. Such simulations were performed using a code written in MatLab and is based on the transfer matrix method. Analysis of the fitting curves allows estimating the refractive index and thus the porosity of the alternated layers, which turns out to be $n_1 \approx 1.85$, $p_1 \approx 40\%$, $n_2 \approx 2.10$, and $p_2 \approx 20\%$. In the case of the structure with broken translational symmetry, the defect layer is of the more porous type. Since dye loading increases with the porosity of the layers, higher absorber concentration is expected in lower refractive index layers.

Incident photon to current efficiency (IPCE) measurements were taken from both multilayers and adequate reference samples. All samples were deposited onto conducting substrates and soaked with a redox electrolyte capable of transporting electrons from the counterelectrode (a platinized conducting substrate) to the dye, and holes in the opposite direction, thus allowing for a close loop of charge transport through the structure. All experimental details are provided as SI. While curves obtained for reference samples show the expected shape for a thin dye sensitized nc-TiO_2 electrode, the photocurrent spectra of multilayers present strongly modified shapes around the spectral region at which resonances are expected to occur (450 nm<λ<550 nm). Multilayered electrodes whose IPCEs are displayed in Figures 3a and 3b were in fact designed to confine light near the spectral region at which the dye absorbs more efficiently. So, the effect of the photon resonance is not so pronounced. However, photocurrent spectrum shape modification is dramatic in samples whose IPCEs are displayed in c and d of Figure 3, for which photonic resonances (shaded regions) are expected to occur further from the photogenerated current spectral maximum of the respective references. In those cases, it is clear that the improvement of performance at specific wavelength ranges is compensated by the strong depletion of photon density occurring at photonic stop band frequencies, resulting in null or worse photovoltaic performance, as it has been theoretically predicted[16] and confirmed experimentally (see the SI where I/V curves of multilayers and references are compared).

Clear evidence of resonant photocurrent generation is observed in all cases when experimental enhancement factors are compared to simulations of the spatial and spectral distribution of the electric field intensity along the multilayers, as we do in Figure 4, which also serves to shed light on the

dx.doi.org/10.1021/ja401096k | J. Am. Chem. Soc. 2013, 135, 7803−7806

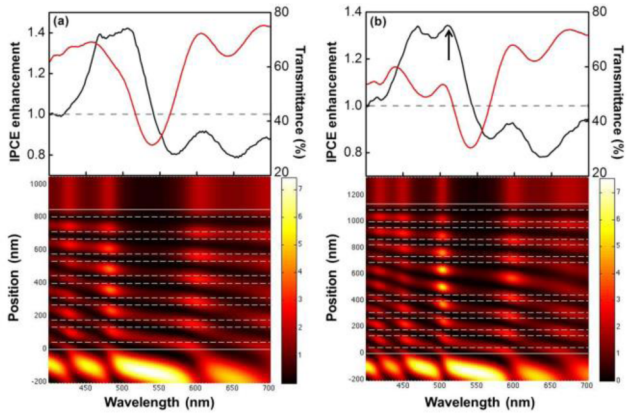

Figure 4. Spectral variation of the photocurrent enhancement factors (black solid lines) for two of the dye-sensitized multilayers whose IPCEs are shown in Figure 3. (a) Periodic arrangement of layers (d_1 = 90 nm, d_2 = 47 nm) and (b) a resonator built by depositing a thicker middle layer within a periodic multilayer (d_1 = 88 nm, d_2 = 44 nm, d_3 = 240 nm). In the bottom panels, the calculated spatial distribution of the electric field along a cross section of both types of structures is plotted as a function of the incident wavelength. Horizontal white dashed lines indicate the position of the interfaces between the two types of titania layers present in the multilayer. In the case of the resonator, the cavity mode is indicated with an arrow. Transmittance spectra are also included for the sake of comparison.

physical mechanism behind these phenomena. Enhancements were estimated as the ratio between the IPCEs of the different types of multilayers under analysis and that of the corresponding reference and calculations were performed using the same code employed to fit the optical transmittance spectra. Both the spectral variation of the observed reinforcement (top graphs, black solid lines) and that of the spatial and spectral distribution of the squared electric field magnitude (bottom images) are plotted in a and b of Figure 4 for a periodic structure and for another in which an optical cavity has been introduced, respectively. Enhancement factors show a strong spectral dependence and reach values up to 40%.

The spectral position and width of photocurrent enhancement peaks (upper panels in Figure 4) coincide fairly well with those of the photon resonances in the nanostructures (lower panels), although it should be kept in mind that enhancement factors are dependent on the properties of the sample chosen as reference. In this regard, it must be pointed out that this choice is actually critical to adequately evaluate the magnitude of the resonant effects herein investigated. We decided to prepare all reference samples using just the more porous titania employed to prepare the photonic crystal, which is the one that can uptake more dye from the solution.

By not using other multilayers as references, we prevent the possibility of having photonic effects in the reference sample that could lead to various artifacts, as it is thoroughly explained in the SI.

References of this kind were prepared with various thicknesses and optically characterized. Since any illuminated thin film gives rise to a non-uniform spatial distribution of the electromagnetic energy density within, we make sure that the spectral regions of localized field intensity in the reference coincide with the photonic resonances observed in the photonic crystal electrodes by modeling the different homogeneous films prepared. By doing so, we avoid the observation of overestimated enhancements. Also, for each reference the amount of dye loaded was controlled to make sure that it was similar to that of the photonic crystal electrode under analysis, which was confirmed by ulterior dye desorption and subsequent colorimetric analysis. Evidence supporting our choice for the reference sample is provided by the fact that the IPCEs are the same at wavelengths for which no photonic effects are expected in the multilayers under study. This can be seen in Figure 3, in which as-measured spectra are shown.

From the analysis of Figure 4, it is clear that certain resonances result in a large enhancement of the photocurrent (like those at λ < 550 nm in both photonic crystal and resonator), while others have no effect or even a deleterious one. These differences can be understood in terms of the particular way in which light frequencies are localized in a periodic nanostructure. Photons with wavelengths coinciding with the "blue edge" of the photonic band gap will localize preferentially in lower dielectric constant layers, that is, those that are more porous and therefore can support a larger amount of dye.[26] So, when light of that wavelength is shone onto the periodic multilayer, the density of electromagnetic energy will be larger in more porous and dye loaded slabs than in denser and less dye sensitized ones. This effect can be clearly seen in the lower panels of a and b of Figure 4, in which dashed white lines indicate the interface between different types of layers (in both selected examples, thinner layers are denser than thicker ones). Hence, the incident photon to collected electron efficiencies of the so-designed multilayers will largely exceed that of the reference at those frequencies. Conversely, for wavelengths at the photonic band gap "red edge", the performance of the multilayer is worse than that of the reference, since in that case light localizes in denser, less dye-loaded layers. Also, poorer photon-to-electron conversion performance is found at photonic gap frequencies, as a result of the blocking of incoming radiation. In the case of the resonator (Figure 4b), the localized field both in the alternated highly porous layers at blue-edge frequencies and in the middle layer at the cavity mode (highlighted with an arrow) gives rise to a double-peak structure in the photocurrent enhancement spectrum.

In order to further show the link between localized photon modes and photocurrent generation resonances, we plot in Figure 5 the angular response of the photonic crystal electrode. Photon resonances, be they band edge or cavity modes, shift toward shorter wavelengths as the angle of incident light increases, as do the corresponding IPCE enhancement maxima detected for both types of structures. The variation of the spectral position of the enhancement peaks observed in each case is plotted against the angle in c and d of Figure 5. This spectral downshift of the field reinforcement maximum is in good agreement with the results of our transfer matrix calculations.

In conclusion, our results demonstrate that arranging nanostructured photoconducting materials in a periodic superstructure provides a means of tailoring the spectral response of the photocurrent. Light confinement effects have been designed to match the desired absorption spectral range and thus selectively enhance the photon-to-electron conversion response. The effect of resonances of different origin (band edge, cavity modes) could be clearly distinguished in the photocurrent spectra of both periodic and broken symmetry optical lattices. These results constitute clear evidence of resonant photocurrent generation in a periodic nanostructure in which a direct relation between resonant photon modes and

dx.doi.org/10.1021/ja401096k | J. Am. Chem. Soc. 2013, 135, 7803−7806

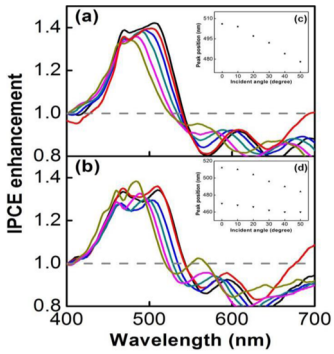

Figure 5. Angular dependence of the photocurrent enhancement spectra for the two dye sensitized multilayers whose enhancement factors are plotted in Figure 4: (a) periodic arrangement of layers and (b) a resonator built by depositing a thicker middle layer within a periodic multilayer. Each color correspond to a different light incident angle, namely, 0° (black), 10° (red), 20° (blue), 30° (cyan), 40° (magenta), and 50° (dark yellow). The angular variation of the photocarrier generation maximum wavelength is plotted for both the periodic and the optical cavity structures in (c) and (d), respectively.

photon-to-electron conversion peaks can be established. We foresee this sort of structure could allow the development of photoelectrochemical devices with finer spectral control over light absorption.

■ ASSOCIATED CONTENT

Supporting Information

Details on the synthesis of TiO_2 particles and multilayers, the assembly of photonic TiO_2 electrodes; details on the optical and the photoelectrochemical experiments; examples of optimized fittings of transmittance optical spectra and the photovoltaic performance of the multilayers; a thorough comment on the criteria followed to choose the reference electrodes employed. This material is available free of charge via the Internet at http://pubs.acs.org.

■ AUTHOR INFORMATION

Corresponding Author

h.miguez@csic.es

Notes

The authors declare no competing financial interest.

■ ACKNOWLEDGMENTS

The research leading to these results has received funding from the European Research Council under the European Union's Seventh Framework Programme (FP7/2007−2013)/ERC grant agreement n° 307081 (POLIGHT), the Spanish Ministry of Economy and Competitiveness under grants MAT2011−23593 and CONSOLIDER HOPE CSD2007−00007, and the Junta de Andalucía under grants FQM3579 and FQM5247.

■ REFERENCES

(1) Macleod, H. A. *Thin Film Optical Filters*, 3rd ed.; Institute of Physics Publishing: London, 2001.
(2) Sakoda, K. *Optical Properties of Photonic Crystals*; Springer−Verlag, Berlin, 2001.
(3) Law, M.; Greene, L. E.; Johnson, J. C.; Saykally, R.; Yang, P. D. *Nat. Mater.* **2005**, *4*, 455−459.
(4) Anger, P.; Bharadwaj, P.; Novotny, L. *Phys. Rev. Lett.* **2006**, *96*, 113002.
(5) Wu, Z.; Lee, D.; Rubner, M. F.; Cohen, R. E. *Small* **2007**, *3*, 1445−1451.
(6) Choi, S. Y.; Mamak, M.; von Freymann, G.; Chopra, N.; Ozin, G. A. *Nano Lett.* **2006**, *6*, 2456−2461.
(7) Fuertes, M. C.; López-Alcaraz, F. J.; Marchi, M. C.; Troiani, H. E.; Míguez, H.; Soler Illia, G. J. A. A. *Adv. Funct. Mater.* **2007**, *17*, 1247−1254.
(8) Colodrero, S.; Ocaña, M.; Míguez, H. *Langmuir* **2008**, *24*, 4430−4434.
(9) Chen, J. I. L.; von Freymann, G.; Choi, S. Y.; Kitaev, V.; Ozin, G. A. *Adv. Mater.* **2006**, *18*, 1915−1919.
(10) Nishimura, S.; Abrams, N.; Lewis, B. A.; Halaoui, L. I.; Mallouk, T. E.; Benkstein, K. D.; van de Lagemaat, J.; Frank, A. J. *J. Am. Chem. Soc.* **2003**, *125*, 6306−6310.
(11) Chen, X.; Ye, J.; Ouyang, S.; Kako, T.; Li, Z.; Zou, Z. *ACS Nano* **2011**, *5*, 4310.
(12) Guldin, S.; Hüttner, S.; Kolle, M.; Welland, M. E.; Müller-Buschbaum, P.; Friend, R. H.; Steiner, U.; Tétreault, N. *Nano Lett.* **2010**, *10*, 2303.
(13) Chen, H.; Chen, S.; Quan, X.; Zhang, Y. *Environ. Sci. Technol.* **2010**, *44*, 451−455.
(14) Sordello, F.; Duca, C.; Maurinoa, V.; Minero, C. *Chem. Commun.* **2011**, *47*, 6147−6149.
(15) Wu, M.; Li, Y.; Deng, Z.; Su, B. L. *ChemSusChem* **2011**, *4*, 1481.
(16) Mihi, A.; Míguez, H. *J. Phys. Chem. B* **2005**, *109*, 15968−15976.
(17) Halaoui, L. I.; Abrams, N. M.; Mallouk, T. E. *J. Phys. Chem. B* **2005**, *109*, 6334−6342.
(18) Chen, J. I. L.; von Freymann, G.; Kitaev, V.; Ozin, G. A. *J. Am. Chem. Soc.* **2007**, *129*, 1196−1202.
(19) Steele, J. J.; van Popta, A. C.; Hawkeye, M. M.; Sit, J. C.; Brett, M. J. *Sens. Actuators B* **2006**, *120*, 213−219.
(20) Guo, D. L.; Fan, L. X.; Wang, F. H.; Huang, S. Y.; Zou, X. W. *J. Phys. Chem. C* **2008**, *112*, 17952−17956.
(21) Schubert, M. F.; Xi, J. Q.; Kim, J. K.; Schubert, E. F. *Appl. Phys. Lett.* **2007**, *90*, 141115.
(22) Calvo, M. E.; Colodrero, S.; Rojas, T. C.; Anta, J. A.; Ocaña, M.; Míguez, H. *Adv. Funct. Mater.* **2008**, *18*, 2708−2715.
(23) Guldin, S.; Kolle, M.; Stefik, M.; Langford, R.; Eder, D.; Wiesner, U.; Steiner, U. *Adv. Mater.* **2011**, *23*, 3664−3668.
(24) Chen, X.; Ye, J.; Ouyang, S.; Kako, T.; Li, Z.; Zou, Z. *ACS Nano* **2011**, *5*, 4310−4318.
(25) O'Regan, B.; Grätzel, M. *Nature* **1991**, *353*, 737−740.
(26) A full discussion of this effect is out of the scope of this manuscript, but for those readers interested in the physical origin of the preferential localization of high- and low-frequency modes in, respectively, low and high dielectric constant layers in a Bragg stack we refer the reader toJoannopoulos, J. D.; Meade, R. D.; Winn, J. N. *Photonic Crystals*; Princeton University Press: Princeton, NJ, 1995.